Aerosol Science and Technology

ISSN: (Print) (Online) Journal homepage: https://www.tandfonline.com/loi/uast20

Multi-modal chemical characterization of highly viscous submicrometer organic particles

Ana C. Morales, Brianna N. Peterson, Steven A. L. Sharpe, Shelby M. Huston, Jay M. Tomlin, Felipe A. Rivera-Adorno, Ryan C. Moffet, Alla Zelenyuk & Alexander Laskin

To cite this article: Ana C. Morales, Brianna N. Peterson, Steven A. L. Sharpe, Shelby M. Huston, Jay M. Tomlin, Felipe A. Rivera-Adorno, Ryan C. Moffet, Alla Zelenyuk & Alexander Laskin (05 Oct 2023): Multi-modal chemical characterization of highly viscous submicrometer organic particles, Aerosol Science and Technology, DOI: 10.1080/02786826.2023.2266494

To link to this article: https://doi.org/10.1080/02786826.2023.2266494

AEROSOL SCIENCE AND TECHNOLOGY
https://doi.org/10.1080/02786826.2023.2266494

Multi-modal chemical characterization of highly viscous submicrometer organic particles

Ana C. Morales[a], Brianna N. Peterson[a], Steven A. L. Sharpe[a], Shelby M. Huston[a], Jay M. Tomlin[a]*, Felipe A. Rivera-Adorno[a], Ryan C. Moffet[b], Alla Zelenyuk[c], and Alexander Laskin[a,d]

[a]Department of Chemistry, Purdue University, West Lafayette, Indiana, USA; [b]Sonoma Technology, Inc, Petaluma, California, USA; [c]Atmospheric Sciences and Global Change Division, Pacific Northwest National Laboratory, Richland, Washington, USA; [d]Department of Earth, Atmospheric and Planetary Sciences, Purdue University, West Lafayette, Indiana, USA

ABSTRACT

Distinguishing highly viscous organic particles within complex mixtures of atmospheric aerosol and accurate descriptions of their composition, size distributions, and mixing states are challenges at the forefront of aerosol measurement science and technology. Here, we present results obtained from complementary single-particle measurement techniques employed for the in-depth characterization of highly viscous particles. We demonstrate advantages and synergy of this multi-modal particle characterization approach based on the analysis of individual viscous particles formed in the air-discharged waste produced by a common sewer pipe rehabilitation technology. Using oil immersion flow microscopy, we investigate particle size distributions and morphology of colloidal components present in field-collected aqueous waste condensates. We compare these results with corresponding measurements of viscous particles formed in drying droplets of the aerosolized discharged waste. The colloidal components and viscous particles were found to be approximately 10 μm and 0.5 μm, respectively. The aerosolized viscous particles exhibited a spherical morphology, while the colloidal particles appeared noticeably fractal, resembling fragments of a cured composite material. Chemical imaging of the viscous particles collected on substrates was performed using scanning electron microscopy and soft X-ray spectro-microscopy techniques. Through these methods, comprehensive description of these particles emerged, confirming their high solid-like viscosity, wide-ranging sizes, diverse carbon speciation with high degrees of oxygenation, and high organic volume fractions. The aerosolized viscous particles were further characterized using high-throughput single particle mass spectrometry. This technique provides real-time measurements of composition, size, and morphological metrics for large numbers of individual particles, enabling the identification of their distinct mass spectrometric signatures.

ARTICLE HISTORY
Received 3 August 2023
Accepted 27 September 2023

EDITOR
Jingkun Jiang

CONTACT Alexander Laskin alaskin@purdue.edu Department of Chemistry, Purdue University, 760 Oval Drive, West Lafayette, IN 47906, USA.
*Current affiliation: Earth Science Division, NASA Ames Research Center, Moffett Field, California, USA.

Supplemental data for this article can be accessed online at https://doi.org/10.1080/02786826.2023.2266494.

GRAPHICAL ABSTRACT

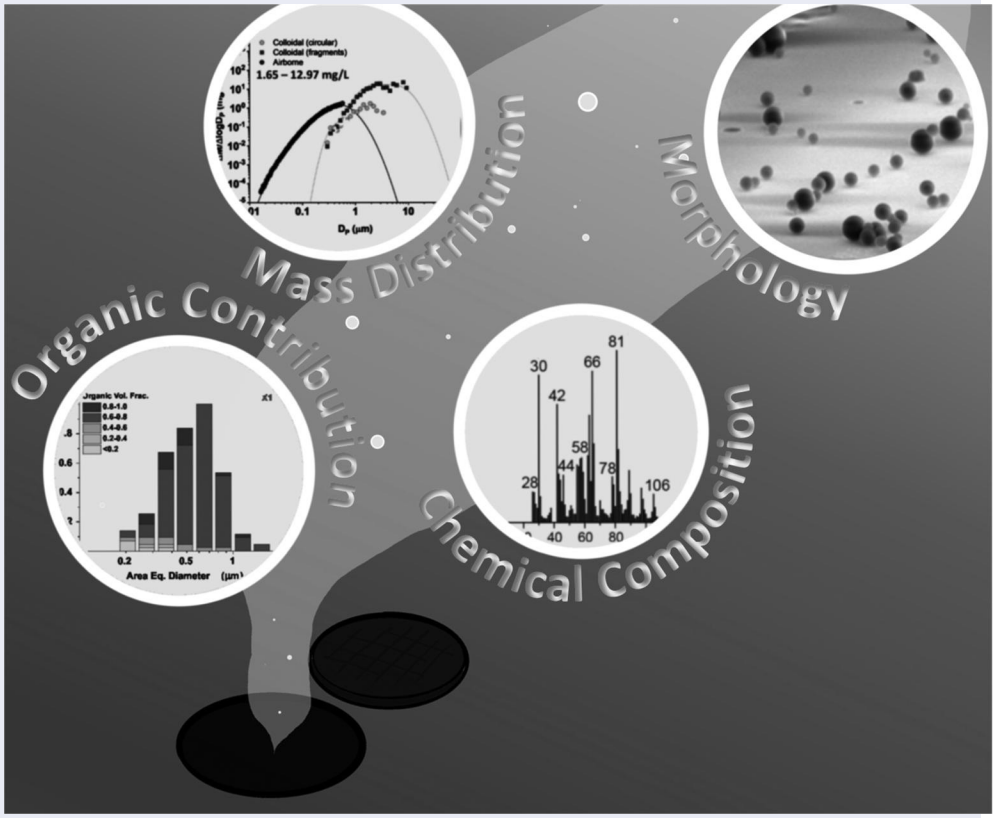

Introduction

Atmospheric organic aerosols (OA) comprise particles emitted directly from primary sources (POA) or formed secondarily (SOA) through oxidation and subsequent condensation of volatile organic compounds (VOCs). OA represents 20% to 95% of total aerosol mass across urban and remote regions (Zhang et al. 2007, 2022; De Gouw and Jimenez 2009; Andreae and Crutzen 1997; Saxena and Hildemann 1996). The size and composition of OA play an important role in determining their physicochemical properties, which have further implications for various environmental factors including visibility, climate, air quality, and human health (Ziemann and Atkinson 2012; Andreae and Rosenfeld 2008; Davidson, Phalen, and Solomon 2005; Lohmann and Feichter 2005; Pöschl 2005; Ramanathan et al. 2001; Haywood and Boucher 2000). The viscosity of aerosol particles is essential when assessing their atmospheric impacts (Shiraiwa et al. 2017; Bateman et al. 2016; Shiraiwa and Seinfeld 2012; Koop et al. 2011). Particle size and viscosity impact the ability of OA to act as cloud condensation nuclei and ice nuclei, where solid particles are more likely to promote ice formation, affecting the global hydrological cycle (Ignatius et al. 2016; Mülmenstädt et al. 2015; Wang et al. 2012; Shiraiwa et al. 2011). Additionally, viscosity of particles influences their growth rate and equilibration times, as viscous particles undergo slower heterogeneous reactions, which ultimately leads to prolonged aging processes (Reid et al. 2018; Shiraiwa et al. 2013; Koop et al. 2011; Wang and Knopf 2011; Mikhailov et al. 2009). The presence of highly viscous particles, often displaying glass-like characteristics and unique chemical composition, were found to be attributed to various sources. Recent reports have identified highly viscous OA from both biogenic and anthropogenic sources. These include glassy SOA from biogenic precursors (Baboomian et al. 2022; Virtanen et al. 2010), solid organic particles from raindrop impaction on soil surfaces (Wang et al. 2016), and solid organic microplastics from common sewer pipe repair technologies (Morales et al. 2022). However, these highly viscous OA categories remain incompletely understood because of challenges of their experimental detection and characterization.

Offline techniques can be used for bulk analysis of the molecular-level components or the chemical imaging of individual particles. Bulk molecular analysis

techniques offer an overall characterization of chemical components in complex OA mixtures. However, they cannot systematically analyze individual particles. Optical microscopy is a minimally destructive method that permits the visualization of micrometer-sized particles. It is often coupled to vibrational spectroscopy techniques, such as Raman or Fourier transform infrared (FTIR), to gain insights into the molecular composition within individual particles (Laskin, Moffet, and Gilles 2019). Although FTIR provides molecular fingerprints, it is susceptible to spectral interferences from water present in ambient OA particles. In contrast, Raman spectroscopy is less influenced by water, rendering it a suitable choice for water-containing OA particles (Bumbrah and Sharma 2016). Both of these techniques are nondestructive and require minimal sample preparation (Cai et al. 2021; Kusch 2020). These techniques are complementary to each other because vibrational modes that are not Raman active are typically active in the infrared and vice versa. However, they lack detailed information about particle morphology and heterogeneity if employed without complementary microscopy methods (Cai et al. 2010, 2021). Chemical imaging by spectro-microscopy techniques provides intricate information at the single-particle level, which allows highly viscous OA to be distinguished from liquid-like OA particles (Liu et al. 2021; Laskin et al. 2016). Specifically, particle size, morphology, and internal components can be imaged using scanning electron microscopy (SEM) and transmission electron microscopy (TEM) (Pósfai and Buseck 2010; Laskin, Cowin, and Iedema 2006). When coupled with energy dispersive X-ray microanalysis, quantitative analysis of particle elemental compositions is achieved (Laskin, Moffet, and Gilles 2019). However, methods of electron microscopy induce beam damage to particles and provide no information about molecular composition (Laskin, Moffet, and Gilles 2019).

Synchrotron-based scanning transmission x-ray microscopy (STXM) coupled to near edge x-ray absorption fine structure (NEXAFS) spectroscopy is a powerful method used to delve into the speciation of specific elements within atmospheric particles commonly used to delve into the speciation of specific elements within atmospheric particles (Moffet, Tivanski, and Gilles 2010b; Kilcoyne et al. 2003; Kirz et al. 1992). With a spatial resolution of ~25 nm, this technique provides insights into the chemical heterogeneity, functionality, mixing states, and size of individual particles (Laskin, Moffet, and Gilles 2019; O'Brien et al. 2014; Moffet, Tivanski, and Gilles 2010b).

Chemical composition of airborne viscous OA particles can be interrogated in-situ by using various aerosol mass spectrometers. These instruments employ rapid volatilization or/and ablation of particles followed by various ionization approaches, causing extensive fragmentation of analyte ions that complicates spectra interpretation (Zhou et al. 2020; Aiken et al. 2009; Nash, Baer, and Johnston 2006). While in-situ aerosol mass spectrometry techniques are favored in field studies, highly viscous OA particles (Morales et al. 2022; Wang et al. 2016) are often highly refractory and cannot be detected efficiently by evaporation-based methods. Laser-ablation based single-particle mass spectrometers allow characterization of both refractory and non-refractory particle components; however, interpretation of particle mass spectra remains difficult due to significant analyte fragmentation (Cai et al. 2015; Zelenyuk et al. 2015; Zelenyuk and Imre 2009).

Because no single technique can simultaneously provide particle size, morphology, shape, molecular composition, and internal heterogeneity, a multi-modal approach becomes essential when investigating solid OA particles. Recently, we have reported that substantial quantity of highly viscous environmental nanoplastic (EnvNP) particles (a subset of the broader defined solid OA particles) could be attributed to direct airborne emissions from a commonly used trenchless technology for storm and sewer pipes repairs (Morales et al. 2022). Here, we present a comprehensive case study and highlight the results of single-particle chemical analysis of EnvNP particles using a multi-modal approach. Colloidal and airborne particle concentrations were estimated based on the measurements provided by the oil immersion flow microscopy and condensation particle counting, respectively. Viscosity of the EnvNP particles was assessed through SEM imaging at a tilted angle. STXM/NEXAFS was used to investigate particle compositions, internal heterogeneity, and organic volume fractions. Finally, an online single particle mass spectrometer characterized large ensembles of EnvNP particles.

Experimental methods

Particle samples

Condensed steam-laden waste emissions from 'cured-in-place-pipe' installations were collected in Sacramento, California on August 2016, as described elsewhere by Teimouri Sendesi et al. (2017). A brief summary of the field sites (X1, X2, X4, X5) and the methods of sample collection (Teimouri Sendesi et al.

2017) are included in Supplementary Note 1. Samples X1, X4, and X5 were collected at installation sites employing a styrene-based (S-based) resin and sample X2 was collected at a site employing a low-VOC vinyl ester-based (VE-based) resin (Teimouri Sendesi et al. 2017).

Individual dried aerosol particles were generated from the condensate samples by nebulizing and conditioning aerosol flow in a drying setup. A diagram (Figure S1) and detailed explanation of the experimental setup are included in Supplementary Note 2. Dried particles were collected using a Sioutas cascade impactor with a Leland Legacy air sampling pump (SKC, Inc.) operated at 9.0 L min^{-1}. Particles were collected on two types of microscopy substrates, Si_3N_4 thin film supported by Si wafer frame (Silson Ltd.) and copper 400 mesh TEM grids coated with carbon type-B thin film (Ted Pella, Inc.). The substrates were mounted onto stage C (0.25–0.50 µm) and stage D (<0.25 µm). The collected samples were stored in desiccator cabinets prior to analysis.

Particle size distributions

Particle size distributions (PSD) of colloidal components of the bulk condensate were measured using a FlowCam® Nano instrument (Yokogawa Fluid Imaging Technologies Inc.) operated with the VisualSpreadsheet 5.6.26 software (Fluid Imaging Technologies). The FlowCam® Nano instrument uses oil immersion flow microscopy (Krause et al. 2021; Hasberg et al. 2019) to focus and image colloidal particles as they pass through a flow cell. Details of the experimental methods and representative particle images (Figure S3) are included in Supplementary Note 3 (West et al. 2023). From the acquired images, a shape factor was calculated for each particle. In this study, we utilize the circularity (or isoperimetric quotient) to distinguish between circular and irregular particle morphologies.

The PSDs of dry aerosolized particles were measured using a scanning mobility particle sizer (SMPS) containing a differential mobility analyzer (TSI model no. 3081) interfaced with a condensation particle counter (CPC, TSI model no. 3776). The SMPS-CPC was operated at an aerosol flow rate of 0.3 L min^{-1}, respectively.

Imaging of substrate deposited particles

SEM images of impacted particles were acquired at tilted 80° angle to infer their viscosity. Particles deposited onto an impactor stage experience deformation of their morphology (Tomlin et al. 2020; Wang et al. 2016; O'Brien et al. 2014). Specifically, liquid-like particles will flatten after colliding with the impactor plate, whereas highly viscous organic particles retain their spherical shape. The measurement of the particle height (H) and width (W) imaged at a tilted angle is then used to estimate the particle viscosity based on the ratio of H/W (Rivera-Adorno et al. 2023). In this study, H and W particle metrics were obtained with ImageJ software 1.52a (National Institutes of Health) and estimates of particle viscosity were done based on comparison of the H/W ratio recorded for laboratory generated sugar particle standards with known viscosities (Rivera-Adorno et al. 2023).

STXM/NEXAFS measurements were conducted at Lawrence Berkeley National Laboratory's Advanced Light Source (ALS) on beamline 5.3.2.2. A detailed description of instrument operation is included in Supplementary Note 4 (Kilcoyne et al. 2003). Briefly, a series of STXM images are acquired at different energies of X-rays to generate a three-dimensional "stack" data set providing spectral information from individual pixels of detected particles at the carbon K-edge (~96 energies between 278 to 320 eV, 35 nm spatial resolution, 1 ms dwell time). In addition, we also acquired wider field of view spectral "maps" to accumulate higher statistics among analyzed particles by utilizing a faster data acquisition of STXM images at four key energies at 278 eV (pre-edge), 285.4 eV (C = C), 288.5 eV (-COOH), and 320 eV (post-edge) (15 × 15 µm, 35 nm spatial resolution, 1 ms dwell time) (Moffet et al. 2010a).

Single particle mass spectrometry

Composition and vacuum aerodynamic diameters of individual aerosolized particles were characterized using a single particle mass spectrometer (miniSPLAT) (Zelenyuk et al. 2015; Zelenyuk and Imre 2005). A detailed description of the instrument development and operation is included in Supplementary Note 5 (Zelenyuk et al. 2015). Wet aerosol flow was generated by nebulizing waste condensates and directing aerosol flow through a charcoal-filled drying tube to reduce the presence of VOCs, followed by a silica gel-filled drying tube to remove residual water. Dried particles were then introduced into a 100 L Teflon chamber pre-filled with ultra-high purity air, used to further dry aerosols and reduce particle coagulation. The Teflon chamber

was connected to the inlet of the miniSPLAT mass spectrometer which performed continuous sampling until records of ~5,000 – 10,000 individual particles/ per sample were acquired.

Results and discussion

Figure 1 showcases mass PSD values of both wet colloids (0.3–20 µm) and dry aerosolized particles (0.015–0.6 µm) corresponding to each of the waste condensates. In all four samples, the mean sizes of the wet colloids and dry particles are ~10 µm and ~0.5 µm, respectively. Our previous work (Morales et al. 2022) has shown that the larger particles (>10 µm) resemble fragments of the pipe polymer composite that are likely shed by mechanical forces of pressurized stream blown through the pipe during the installation process. In contrast, smaller particles (<1 µm) are formed from water-soluble organic compounds dissolved in the process, followed by aqueous-phase oligomerization that occurs in the drying droplets of the discharged waste, which results in solid EnvNP particles (Morales et al. 2022). Morphologies of the colloidal particles were determined based on measured circularity of their representative images (Supplementary Note 3). Circular and irregular colloids are distinguished based on their circularity, using a threshold ratio of 0.75 as the discriminator. PSD measurements of the aerosolized submicron particles by SMPS were converted to the mass loading units of mg L^{-1} (aerosol mass per liter of waste condensate, as described in Supplemental Note 2). Figure 1 illustrates quantitative overlap of the mass PSDs measured for the dry airborne particles and the wet colloids. Notably, these sub-micrometer particles remain in the air for extended periods of days to weeks (Hinds 1999), urging systematic investigation of their mass loadings at the source and their physicochemical properties. Quantitative assessments of the total mass loadings of particles generated from

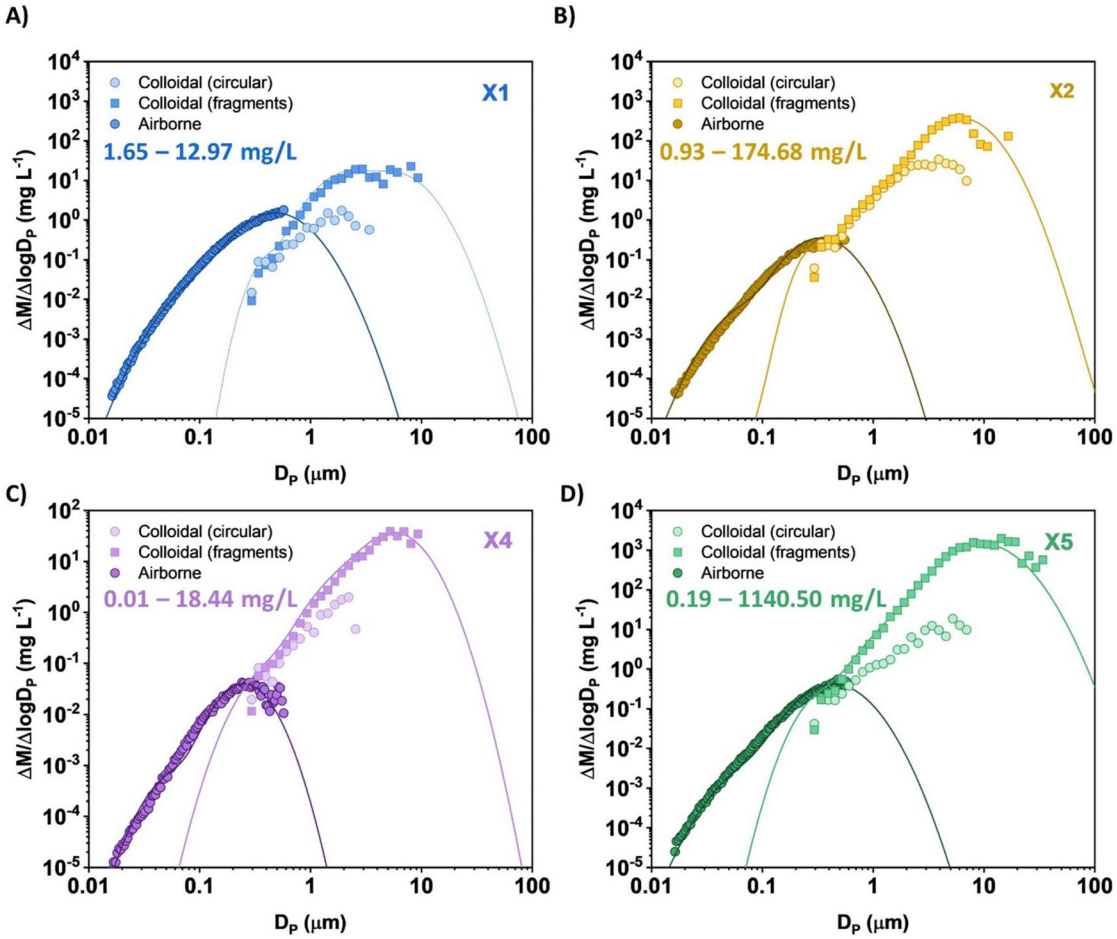

Figure 1. Particle mass size distributions (milligram of solid material per liter of discharged condensate; mg L^{-1}) of wet colloids and dry particles aerosolized from waste condensate samples. Colloids are distinguished based on their observed morphology: circular particles (circles) irregular fragments (squares). Aerosolized particle measurements are reported as dark colored circles. The lines show bi-modal lognormal data fits, and the values represent ranges of the integrated total mass concentrations.

each of four condensates were estimated by integrating the experimental mass PSD data. In this study, the mass PSDs of colloidal particles were used as the upper-level estimate and the mass PSDs of dry particles served as the lower-level estimates. These estimates suggest that between 0.01 and 1140.50 mg L^{-1} of particles per discharged waste condensate are plausibly emitted. Importantly, a significant fraction of these particles falls within the submicrometer size range (Figure S2), capable of lingering airborne for weeks (Hinds 1999).

The high viscosity of the dry particles generated from waste condensates was confirmed by their spherical shape retained after impaction onto the sampling substrates. Figure 2a shows representative SEM images, acquired at a tilt angle of 80°, of dry particles generated from each of four waste samples deposited on the impaction plates. Measured morphology metrics, *H* and *W*, acquired at a tilted angle provide practical metrics for the viscosity assessment. Figure 2b shows particles' *H* versus *W* values, together with the reference lines of different viscosity values indicating that dry particles generated in our experiments have viscosity of solids $\geq 10^{10}$ Pa s, similar to plastic materials (Reid et al. 2018). These particles, previously termed as EnvNP (Morales et al. 2022), resemble the spherical morphology and viscosity exhibited by other solid atmospheric organic particles, such as tar balls (Hand et al. 2005), soil organic particles (Wang et al. 2016), and solid biogenic organic particles (Virtanen et al. 2010). Highly viscous aerosol may serve as a surface for condensation of semi-volatile organic compounds during their atmospheric lifetime and transport (Shiraiwa et al. 2011). These newly formed EnvNP particles can act as nuclei for SOA formation and transport chemicals from the emission source to remote regions due to their long atmospheric lifetimes. Furthermore, EnvNP may have important implications for air quality and visibility, with long-term impacts on climate and human health.

Computer-controlled SEM imaging coupled to the energy dispersive X-ray spectroscopy (CCSEM-EDX) microanalysis of large ensembles of individual EnvNP particles reported in our previous work (Morales et al. 2022), showed their predominantly carbonaceous composition (>75% by particle count). In addition, carbonaceous particles with contributions from mostly Na, Al and Si elements were also detected, which likely reflect inorganic additives of the pipe polymer composite, such as soda ash (Na_2CO_3) and aluminum silicate fibers (mixtures of Al_2O_3 and SiO_2), used to maintain desired consistency and viscosity of the composite. In this study, we delve deeper into the specific chemical bonding of the EnvNP carbonaceous material using STM/NEXAFS, a technique that offers high lateral resolution. Figure 3 shows the carbon K-edge 'maps' of EnvNP particles acquired in STXM experiments. Individual pixels of particle images are colored by overlapping spectral characteristics based on the applied threshold definitions (Moffet et al. 2010a) of 'organic carbon' – OC (green), 'sp^2 hybridized carbon' (red), and 'inorganic components' – IN (blue). The inorganic components are likely metals present in the resin material (Morales et al. 2023; Peterson et al. 2023).

Particle maps shown in Figure 3 were utilized to compute the organic volume fractions (OVF) of

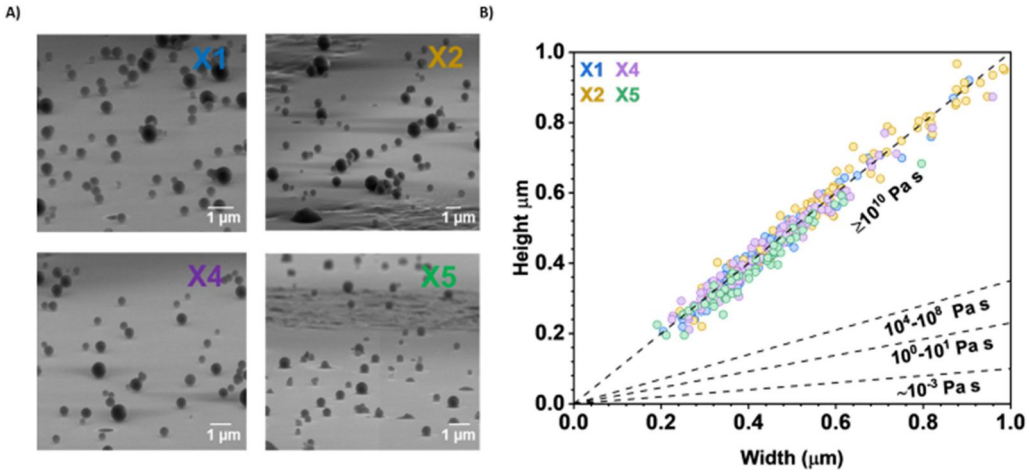

Figure 2. Size, morphology, and viscosity characteristics of dry particles aerosolized from four samples of waste condensate. (a) SEM images (in the secondary electron mode) of particles imaged at 80° tilt angle. Particles with high viscosity remain spherical after impaction; liquid-like particles exhibit flat morphology. (b) Plot of particles observed heights (*H*) versus their width (*W*) observed for particles of this study in reference to standards with known viscosity. Values corresponding to occasional flat (low viscosity) particles, as those seen in X5 image, are not included in the plot for clarity. Viscosity characteristics of individual particles are inferred from comparison to the reference lines.

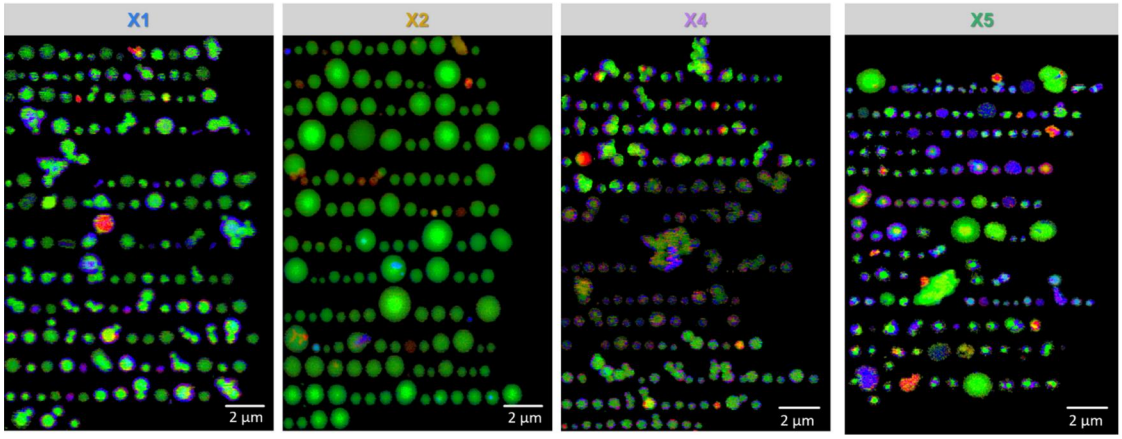

Figure 3. Representative carbon K-edge speciation maps recorded by X-ray spectro-microscopy. Colors correspond to experimentally defined basic chemical components: green – 'organic carbon'; red – 'sp^2 carbon' (indicative of π-bonds network); and blue – 'inorganic components'. The RGB layers are transparent and overlap.

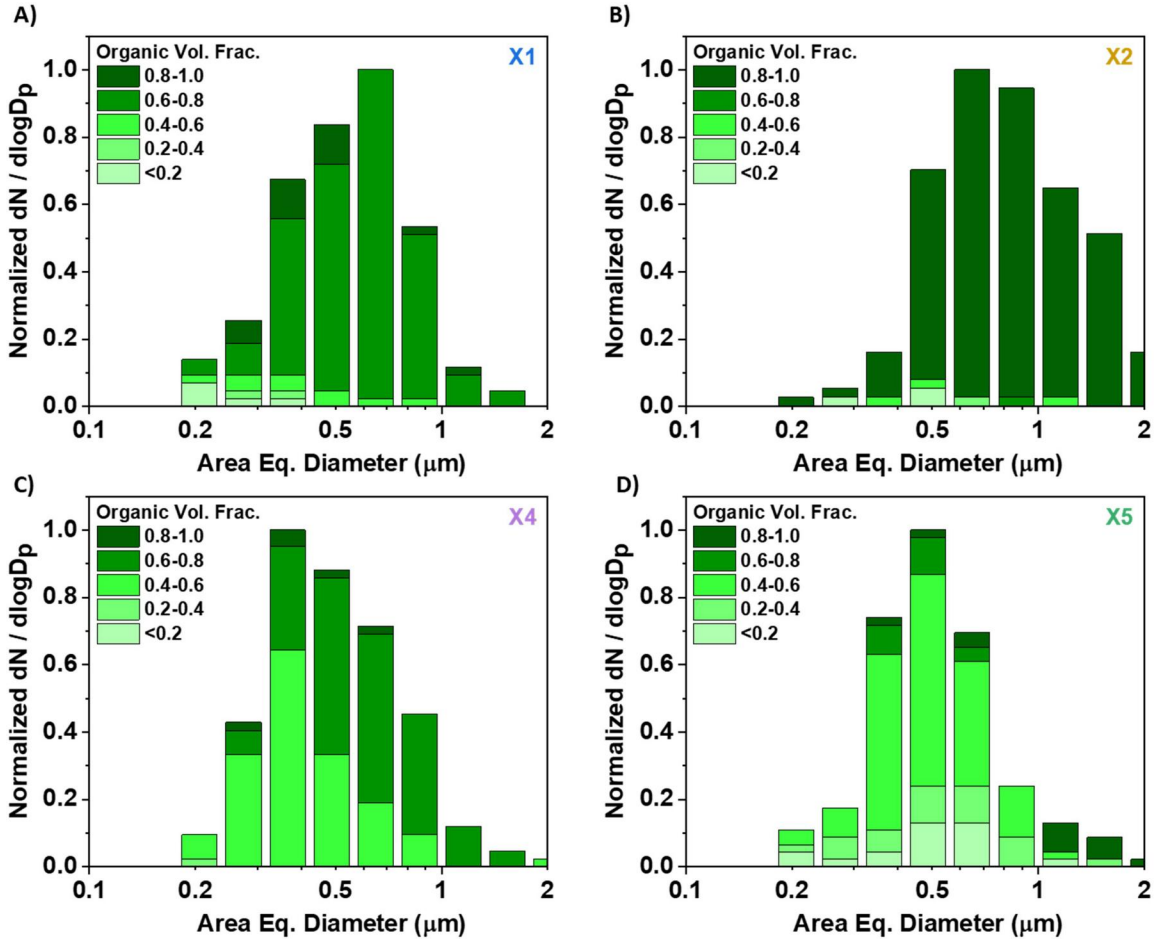

Figure 4. STXM-derived organic volume fraction (OVF) of individual particles summarized as normalized histograms, size-resolved as 8 bins per decade.

individual particles, employing previously established methodology (Fraund et al. 2019) summarized in Supplementary Note 4. The OVF values are used to assess reactivity and hygroscopicity of particles, which also influence particle size, chemical composition, and internal distribution of components (Wu et al. 2016; Schill et al. 2015; Folkers, Mentel, and Wahner 2003; Worsnop et al. 2002). Figure 4 shows the size-resolved OVF values of EnvNP particles acquired from STXM/NEXAFS maps. Across all four samples, the majority

of particles exhibit organic components contributing to more than 50% of the total volume. Notably, particles generated from the VE-based condensate (X2) have substantially higher fractions of particles with OVF >80%. This is plausibly a result of the VE-based resin composition, where the resin contains a higher concentration of lower volatility organic components than the S-based resin. This aligns with the molecular characterization of this sample, which demonstrated an increased presence of condensed organic materials discussed in a separate report (Morales et al. 2023).

The NEXAFS spectra of individual EnvNP particles extracted from STXM 'stacks' were used to investigate the chemical bonding environment of carbon. Figure 5 displays the NEXAFS spectra of selected individual particles and their associated STXM images, representative of EnvNP particles obtained from each of four condensate samples. Additional NEXAFS spectra of EnvNP particles retrieved from all 'stacks' data

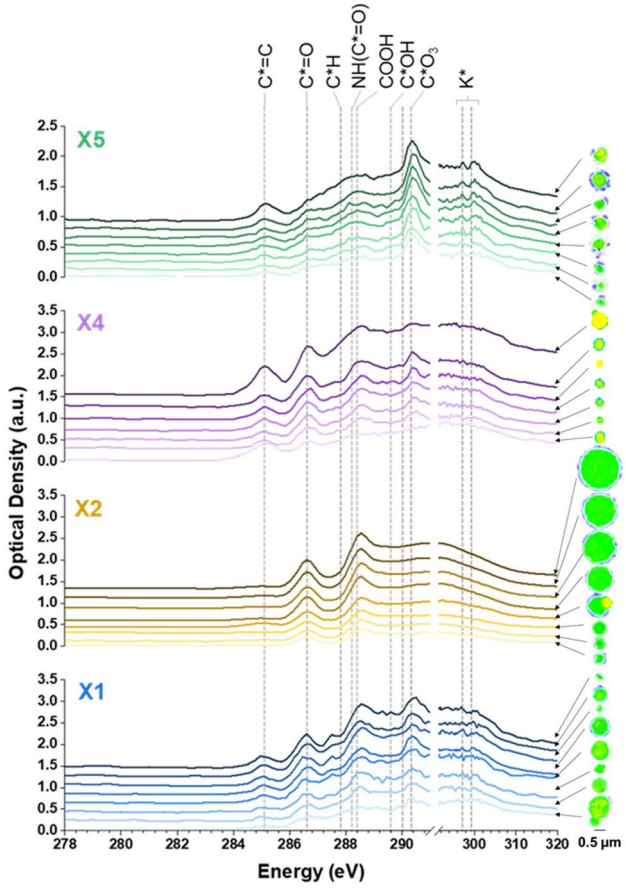

Figure 5. Carbon K-edge spectra of representative individual solid EnvNP particles shown in groups for each of four samples. Areas in the corresponding individual particle maps indicate 'organic carbon' (green), 'sp^2 carbon' (red), and 'inorganic content' (blue) that overlap for some particles. In each of the groups, particle spectra are offset along Y-axis for clarity. Dashed lines indicate absorption by various carbon-containing groups and potassium, as indicated by the legends.

sets of this study are presented in Supplementary Note 4, Figure S4. The deconvolution fits of the averaged NEXAFS spectra for the four samples are presented in Figure S5. If observed EnvNP particles were fragments of the polystyrene polymer composite from the S-based resin operation (X1,4,5), their spectra would exhibit dominant alkene features of C* = C at 284.9 eV. However, it's noteworthy that the 284.9 eV feature is very weak compared to other carbon bonding features observed in these particles. Across all samples, the most abundant feature corresponds to the alcohol groups (C*-OH at 289.5 eV), accompanied by discernible features corresponding to carbonyl (C* = O at 286.7 eV) and carboxylate (COOH at 288.5 eV) groups. This profile suggests that the OC components of the EnvNP particles are significantly oxygenated hydrocarbons, plausibly oligomeric products formed in drying microdroplets of the waste condensates (Morales et al. 2022). Notably, there is variability between individual particles in the three S-based samples, likely resulting from uncontrolled multi-phase oligomeric reactions that occur in the emission plume (Morales et al. 2022; Herrmann et al. 2015; Zhao et al. 2013; Nguyen et al. 2011; Ziemann 2003; Kimura 1998). This observation aligns with our other report (Peterson et al. 2023), which indicated that these particles do not resemble the starting resin material or the intended cured composite composition, implying uncontrolled reactions in the drying waste microdroplets.

The chemical composition of the individual aerosolized particles was also interrogated by miniSPLAT. In Supplementary Note 5, the average normalized mass spectra (Figure S6) and vacuum aerodynamic diameter PSDs for each of the four samples are presented. The average mass spectra of the samples reveal $^{23}Na^+$, $^{39/41}K^+$, $^{81/83}Na_2Cl^+$ ions that correspond to soluble inorganic components. The higher potassium content observed in samples X1 and X5 is consistent with the corresponding NEXAFS spectra (Figure S4). Inspection of mass spectral features related to organic fraction (Figure S7) points to the presence of fragment ions previously observed in the laboratory-generated styrene-based resin and composite microplastic particles (Peterson et al. 2023), including $^{78}C_6H_6+$, $^{92}C_7H_8^+$, $^{106}C_7H_6O^+$, $^{42}C_3H_6^+$. However, the VE-based sample (X2) stands out with an average mass spectrum distinct from those of the laboratory-generated vinyl-based resin and composite microplastic particles (Peterson et al. 2023). Notably, the vacuum aerodynamic diameter PSDs for the four waste condensate samples (Figure S7) show that particles

generated from X2 and X4 samples had the largest and smallest sizes, respectively, in line with the X-ray microscopy data presented in Figure 4.

To facilitate data interpretation, the miniSPLAT characterization provides chemical composition insights into thousands of individual particles, which were categorized by an unsupervised classification algorithm (Zelenyuk et al. 2015) into six distinct particle classes based on the similarity of their mass spectra. Figure 6a shows the relative contribution of the six identified particle classes across the four samples. The average mass spectra of particles classified into these classes (Figure 6b) show that while particles from classes 2, 3, and 5 exhibit mass spectral features reminiscent of the laboratory-generated styrene-based resin and composite microplastic particles (Peterson et al. 2023), particles from classes 1, 4, and 6 have distinctly dissimilar mass spectra. Furthermore, samples X1, X2 and X4 are dominated by particles from classes 2, 3, and 5. However, sample X5 contains the largest fraction of particles with mass spectra that do not exhibit signatures of microplastic, consistent with the higher fraction of inorganic content in the particles observed in Figure 2a.

Conclusions and implications

The comprehensive multi-modal analytical approach implemented in this study offers a detailed chemical profiling of EnvNP particles. This approach can be adopted for future field studies of solid OA particles originated from discharged waste discussed here, as well as from natural aquatic environments such as terrestrial and marine surface water containing dissolved and colloidal organic material (Cochran et al. 2017; Wang et al. 2016). The sizes and morphologies of colloidal and dry airborne particles can be quantitatively investigated by combined measurements of oil immersion flow microscope and scanning mobility particle sizer (SMPS), reported as particles concentrations per volume of tested water. EnvNP particles investigated in this study were notably prevalent, with high circularity (>0.75). Presence of solid (highly viscous) OA particles and their fraction out of the total aerosol population can be detected and quantified in real time using field-deployable impactor apparatus that counts particles rebound (Bateman, Belassein, and Martin 2014) between the stages. Alternatively, SEM imaging of impacted particles imaged at tilted angle can unveil their highly viscous, spherical nature. Offline STXM chemical imaging can uniquely identify individual solid OA particles out of larger particles ensembles based on their substantially higher optical depth and preserved spherical morphology (Morales et al. 2022; Fraund et al. 2020; Tomlin et al. 2020; Wang et al. 2016). Their corresponding NEXAFS spectral features can be quantified to yield OVF values and particle mixing state metrics, as well as to evaluate chemical bonding environment of carbon and to compare those with known standard materials and previously observed ambient particles. In this study, the observed exhibited unexpectedly high OVF values and contained oxygenated functional groups, diverging from their intended polymer composition. While off-line chemical imaging by STXM/NEXAFS asserts unique analytical tenets for chemical characterization of solid OA particles, its practical application is constrained by low particle statistics and time-limited access to the synchrotron-based instrumentation. Nevertheless, chemical imaging of individual particles complements and enriches interpretation of data sets acquired by the high-throughput single particle mass spectrometry that can be employed for targeted analysis of solid OA particles in test laboratory experiments and at

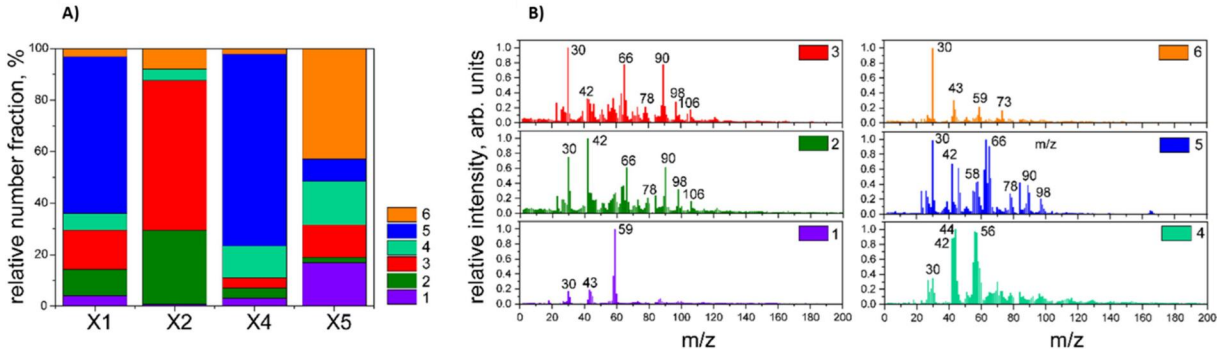

Figure 6. (a) miniSPLAT derived percent contributions of different particle classes based on the total number of particles detected for each sample. (b) Average normalized mass spectra of the six clustered particle classes. MS of individual particles classified in classes 2, 3, and 5 exhibit MS peaks previously observed for the laboratory-generated microplastic particles (e.g., $^{78}C_6H_6+$, $^{92}C_7H_8^+$, $^{106}C_7H_6O^+$, $^{42}C_3H_6^+$).

field sites located close to identified emission sources. Complementary results of these studies, including characteristic mass spectral signatures of microplastic particles identified by single particle mass spectrometry, create fingerprint records of solid OA particles that, in turn, will inform detection of these particles in other field observations, including targeted mining of data from numerous previous studies where large volume of data had been already generated by single particle mass spectrometry.

Acknowledgments

We acknowledge S.M.T. Sendesi, B. E. Boor, J.A. Howarter, Y. Noh, and A. J. Whelton for collection of waste condensate samples used in this study. The authors would like to acknowledge beamline 5.3.2.2 at the Advanced Light Source at Lawrence Berkeley National Laboratory and beamline scientist Matthew Marcus for his support. This work utilized the CCSEM/EDX at the Environmental Molecular Sciences Laboratory at the Pacific Northwest National Laboratory.

Disclosure statement

No potential conflict of interest was reported by the author(s).

Funding

This work was supported by the U.S. National Science Foundation, Grant No. CBET-2107946.

ORCID

Ana C. Morales http://orcid.org/0000-0001-6969-2883
Brianna N. Peterson http://orcid.org/0000-0002-6297-8552
Steven A. L. Sharpe http://orcid.org/0000-0001-7927-2874
Shelby M. Huston http://orcid.org/0009-0000-2195-9219
Jay M. Tomlin http://orcid.org/0000-0002-3081-1512
Felipe A. Rivera-Adorno http://orcid.org/0000-0002-7355-7999
Ryan C. Moffet http://orcid.org/0000-0002-2352-5454
Alla Zelenyuk http://orcid.org/0000-0002-0674-0910
Alexander Laskin http://orcid.org/0000-0002-7836-8417

References

Aiken, A. C., D. Salcedo, M. J. Cubison, J. A. Huffman, P. F. DeCarlo, I. M. Ulbrich, K. S. Docherty, D. Sueper, J. R. Kimmel, D. R. Worsnop, et al. 2009. Mexico City aerosol analysis during MILAGRO using high resolution aerosol mass spectrometry at the urban supersite (T0) – Part 1: Fine particle composition and organic source apportionment. *Atmos. Chem. Phys.* 9 (17):6633–53. doi: 10.5194/acp-9-6633-2009.

Andreae, M. O., and P. J. Crutzen. 1997. Atmospheric aerosols: Biogeochemical sources and role in atmospheric chemistry. *Science.* 276 (5315):1052–8. doi: 10.1126/science.276.5315.1052.

Andreae, M. O., and D. Rosenfeld. 2008. Aerosol–cloud–precipitation interactions. Part 1. The nature and sources of cloud-active aerosols. *Earth-Sci. Rev.* 89 (1–2):13–41. doi: 10.1016/j.earscirev.2008.03.001.

Baboomian, V. J., G. V. Crescenzo, Y. Huang, F. Mahrt, M. Shiraiwa, A. K. Bertram, and S. A. Nizkorodov. 2022. Sunlight can convert atmospheric aerosols into a glassy solid state and modify their environmental impacts. *Proc. Natl. Acad. Sci. USA.* 119 (43):e2208121119. doi: 10.1073/pnas.2208121119.

Bateman, A. P., H. Belassein, and S. T. Martin. 2014. Impactor apparatus for the study of particle rebound: Relative humidity and capillary forces. *Aerosol Sci. Technol.* 48 (1):42–52. doi: 10.1080/02786826.2013.853866.

Bateman, A. P., Z. Gong, P. Liu, B. Sato, G. Cirino, Y. Zhang, P. Artaxo, A. K. Bertram, A. O. Manzi, L. V. Rizzo, et al. 2016. Sub-micrometre particulate matter is primarily in liquid form over Amazon rainforest. *Nature Geosci.* 9 (1):34–7. doi: 10.1038/ngeo2599.

Bumbrah, G. S., and R. M. Sharma. 2016. Raman spectroscopy – Basic principle, instrumentation and selected applications for the characterization of drugs of abuse. *Egypt. J. Forensic Sci.* 6 (3):209–15. doi: 10.1016/j.ejfs.2015.06.001.

Cai, D., A. Neyer, R. Kuckuk, and H. M. Heise. 2010. Raman, mid-infrared, near-infrared and ultraviolet–visible spectroscopy of PDMS silicone rubber for characterization of polymer optical waveguide materials. *J. Mol. Struct.* 976 (1–3):274–81. doi: 10.1016/j.molstruc.2010.03.054.

Cai, H., E. G. Xu, F. Du, R. Li, J. Liu, and H. Shi. 2021. Analysis of environmental nanoplastics: Progress and challenges. *Chem. Eng. J.* 410:128208. doi: 10.1016/j.cej.2020.128208.

Cai, J., M. Zheng, C.-Q. Yan, H.-Y. Fu, Y.-J. Zhang, M. Li, Z. Zhou, and Y.-H. Zhang. 2015. Application and progress of single particle aerosol time-of-flight mass spectrometry in fine particulate matter research. *Chin. J. Anal. Chem.* 43 (5):765–74. doi: 10.1016/S1872-2040(15)60825-8.

Cochran, R. E., O. Laskina, J. V. Trueblood, A. D. Estillore, H. S. Morris, T. Jayarathne, C. M. Sultana, C. Lee, P. Lin, J. Laskin, et al. 2017. Molecular diversity of sea spray aerosol particles: Impact of ocean biology on particle composition and hygroscopicity. *Chem.* 2 (5):655–67. doi: 10.1016/j.chempr.2017.03.007.

Davidson, C. I., R. F. Phalen, and P. A. Solomon. 2005. Airborne particulate matter and human health: A review. *Aerosol Sci. Technol.* 39 (8):737–49. doi: 10.1080/02786820500191348.

De Gouw, J., and J. L. Jimenez. 2009. Organic aerosols in the earth's atmosphere. *Environ. Sci. Technol.* 43 (20):7614–8. doi: 10.1021/es9006004.

Folkers, M., T. Mentel, and A. Wahner. 2003. Influence of an organic coating on the reactivity of aqueous aerosols probed by the heterogeneous hydrolysis of N_2O_5: Organic

coatings and aerosol reactivity. *Geophys. Res. Lett.* 30 (12). doi: 10.1029/2003GL017168.

Fraund, M., D. J. Bonanno, S. China, D. Q. Pham, D. Veghte, J. Weis, G. Kulkarni, K. Teske, M. K. Gilles, A. Laskin, et al. 2020. Optical properties and composition of viscous organic particles found in the Southern Great Plains. *Atmos. Chem. Phys.* 20:11593–606. doi: 10.5194/acp-20-11593-2020.

Fraund, M., T. Park, L. Yao, D. Bonanno, D. Q. Pham, and R. C. Moffet. 2019. Quantitative capabilities of STXM to measure spatially resolved organic volume fractions of mixed organic/inorganic particles. *Atmos. Meas. Tech.* 12 (3):1619–33. doi: 10.5194/amt-12-1619-2019.

Hand, J. L., W. C. Malm, A. Laskin, D. Day, T. Lee, C. Wang, C. Carrico, J. Carrillo, J. P. Cowin, J. Collett, et al. 2005. Optical, physical, and chemical properties of tar balls observed during the Yosemite aerosol characterization study. *J. Geophys. Res.* 110 (D21):D21210. doi: 10.1029/2004JD005728.

Hasberg, A. K. M., S. Bijaksana, P. Held, J. Just, M. Melles, M. A. Morlock, S. Opitz, J. M. Russell, H. Vogel, and V. Wennrich. 2019. Modern sedimentation processes in Lake Towuti, Indonesia, revealed by the composition of surface sediments. *Sedimentology.* 66 (2):675–98. doi: 10.1111/sed.12503.

Haywood, J., and O. Boucher. 2000. Estimates of the direct and indirect radiative forcing due to tropospheric aerosols: A review. *Rev. Geophys.* 38 (4):513–43. doi: 10.1029/1999RG000078.

Herrmann, H., T. Schaefer, A. Tilgner, S. A. Styler, C. Weller, M. Teich, and T. Otto. 2015. Tropospheric aqueous-phase chemistry: Kinetics, mechanisms, and its coupling to a changing gas phase. *Chem. Rev.* 115 (10):4259–334. doi: 10.1021/cr500447k.

Hinds, W. C. 1999. Uniform particle motion: Settling velocity and mechanical mobility. In *Aerosol technology: Properties, behavior, and measurement of airborne particles*, 46–8. New York: Wiley.

Ignatius, K., T. B. Kristensen, E. Järvinen, L. Nichman, C. Fuchs, H. Gordon, P. Herenz, C. R. Hoyle, J. Duplissy, S. Garimella, et al. 2016. Heterogeneous ice nucleation of viscous secondary organic aerosol produced from ozonolysis of α-pinene. *Atmos. Chem. Phys.* 16 (10):6495–509. doi: 10.5194/acp-16-6495-2016.

Kilcoyne, A. L. D., T. Tyliszczak, W. F. Steele, S. Fakra, P. Hitchcock, K. Franck, E. Anderson, B. Harteneck, E. G. Rightor, G. E. Mitchell, et al. 2003. Interferometer-controlled scanning transmission X-ray microscopes at the advanced light source. *J. Synchrotron Radiat.* 10 (Pt 2):125–36. doi: 10.1107/S0909049502017739.

Kimura, H. 1998. A simple method for the anionic polymerization of α-carbonyl acids in water. *J. Polym. Sci. A Polym. Chem.* 36 (1):189–93. doi: 10.1002/(SICI)1099-0518(19980115)36:1 < 189::AID-POLA23 > 3.0.CO;2-E.

Kirz, J., H. Ade, C. Jacobsen, C. -. Ko, S. Lindaas, I. McNulty, D. Sayre, S. Williams, X. Zhang, and M. Howells. 1992. Soft x-ray microscopy with coherent x rays (invited). *Rev. Sci. Instrum.* 63 (1):557–63. doi: 10.1063/1.1142705.

Koop, T., J. Bookhold, M. Shiraiwa, and U. Pöschl. 2011. Glass transition and phase state of organic compounds: Dependency on molecular properties and implications for secondary organic aerosols in the atmosphere. *Phys. Chem. Chem. Phys.* 13 (43):19238–55. doi: 10.1039/c1cp22617g.

Krause, N., S. Kuhn, E. Frotscher, F. Nikels, A. Hawe, P. Garidel, and T. Menzen. 2021. Oil-immersion flow imaging microscopy for quantification and morphological characterization of submicron particles in biopharmaceuticals. *Aaps J.* 23 (1):13. doi: 10.1208/s12248-020-00547-9.

Kusch, P. 2020. Challenges in the analysis of micro and nanoplastics. In *Handbook of microplastics in the environment*, ed. T. Rocha-Santos, M. Costa, C. Mouneyrac, 1–26. Cham: Springer International Publishing.

Laskin, A., J. P. Cowin, and M. J. Iedema. 2006. Analysis of individual environmental particles using modern methods of electron microscopy and X-ray microanalysis. *J. Electron Spectrosc. Relat. Phenom.* 150 (2–3):260–74. doi: 10.1016/j.elspec.2005.06.008.

Laskin, A., M. K. Gilles, D. A. Knopf, B. Wang, and S. China. 2016. Progress in the analysis of complex atmospheric particles. *Annu. Rev. Anal. Chem. (Palo Alto Calif.).* 9 (1):117–43. doi: 10.1146/annurev-anchem-071015-041521.

Laskin, A., R. C. Moffet, and M. K. Gilles. 2019. Chemical imaging of atmospheric particles. *Acc. Chem. Res.* 52 (12):3419–31. doi: 10.1021/acs.accounts.9b00396.

Liu, L., J. Zhang, Y. Zhang, Y. Wang, L. Xu, Q. Yuan, D. Liu, Y. Sun, P. Fu, Z. Shi, et al. 2021. Persistent residential burning-related primary organic particles during wintertime hazes in North China: Insights into their aging and optical changes. *Atmos. Chem. Phys.* 21 (3):2251–65. doi: 10.5194/acp-21-2251-2021.

Lohmann, U., and J. Feichter. 2005. Global indirect aerosol effects: A review. *Atmos. Chem. Phys.* 5 (3):715–37. doi: 10.5194/acp-5-715-2005.

Mikhailov, E., S. Vlasenko, S. T. Martin, T. Koop, and U. Pöschl. 2009. Amorphous and crystalline aerosol particles interacting with water vapor: Conceptual framework and experimental evidence for restructuring, phase transitions and kinetic limitations. *Atmos. Chem. Phys.* 9 (24):9491–522. doi: 10.5194/acp-9-9491-2009.

Moffet, R. C., T. Henn, A. Laskin, and M. K. Gilles. 2010a. Automated chemical analysis of internally mixed aerosol particles using X-ray spectromicroscopy at the carbon K-edge. *Anal. Chem.* 82 (19):7906–14. doi: 10.1021/ac1012909.

Moffet, R. C., A. V. Tivanski, and M. K. Gilles. 2010b. Scanning transmission X-ray microscopy: Applications in atmospheric aerosol research. In *Fundamentals and Applications in Aerosol Spectroscopy*, eds. R. Signorell and J. P. Reid, 419−462. United States: Taylor and Francis Books, Inc.

Morales, A. C., J. M. Tomlin, C. P. West, F. A. Rivera-Adorno, B. N. Peterson, S. A. L. Sharpe, Y. Noh, S. M. T. Sendesi, B. E. Boor, J. A. Howarter, et al. 2022. Atmospheric emission of nanoplastics from sewer pipe repairs. *Nat. Nanotechnol.* 17 (11):1171–7. doi: 10.1038/s41565-022-01219-9.

Morales, A. C., C. P. West, B. N. Peterson, Y. Noh, A. J. Whelton, and A. Laskin. 2023. Diversity of organic components in airborne waste discharged from sewer pipes repairs. *Environ. Sci. Process. Impacts.* Advance online publication. doi: 10.1039/D3EM00084B.

Mülmenstädt, J., O. Sourdeval, J. Delanoë, and J. Quaas. 2015. Frequency of occurrence of rain from liquid-, mixed-, and ice-phase clouds derived from a-train satellite retrievals. *Geophys. Res. Lett.* 42 (15):6502–9. doi: 10.1002/2015GL064604.

Nash, D. G., T. Baer, and M. V. Johnston. 2006. Aerosol mass spectrometry: An introductory review. *Int. J. Mass Spectrom.* 258 (1–3):2–12. doi: 10.1016/j.ijms.2006.09.017.

Nguyen, T. B., P. J. Roach, J. Laskin, A. Laskin, and S. A. Nizkorodov. 2011. Effect of humidity on the composition of isoprene photooxidation secondary organic aerosol. *Atmos. Chem. Phys.* 11 (14):6931–44. doi: 10.5194/acp-11-6931-2011.

O'Brien, R. E., A. Neu, S. A. Epstein, A. C. MacMillan, B. Wang, S. T. Kelly, S. A. Nizkorodov, A. Laskin, R. C. Moffet, and M. K. Gilles. 2014. Physical properties of ambient and laboratory-generated secondary organic aerosol: Physical properties of organic aerosol. *Geophys. Res. Lett.* 41 (12):4347–53. doi: 10.1002/2014GL060219.

Peterson, B. N., A. C. Morales, J. M. Tomlin, C. G. W. Gorman, P. E. Christ, S. A. L. Sharpe, S. M. Huston, F. A. Rivera-Adorno, B. T. O'Callahan, M. Fraund, et al. 2023. Chemical characterization of nanoplastic particles formed in airborne waste discharged from sewer pipe repairs. *Environ. Sci. Process. Impacts*. Advance online publication. doi: 10.1039/D3EM00193H.

Pöschl, U. 2005. Atmospheric aerosols: Composition, transformation, climate and health effects. *Angew. Chem. Int. Ed. Engl.* 44 (46):7520–40. doi: 10.1002/anie.200501122.

Pósfai, M., and P. R. Buseck. 2010. Nature and climate effects of individual tropospheric aerosol particles. *Annu. Rev. Earth Planet. Sci.* 38 (1):17–43. doi: 10.1146/annurev.earth.031208.100032.

Ramanathan, V., P. J. Crutzen, J. T. Kiehl, and D. Rosenfeld. 2001. Aerosols, climate, and the hydrological cycle. *Science.* 294 (5549):2119–24. doi: 10.1126/science.1064034.

Reid, J. P., A. K. Bertram, D. O. Topping, A. Laskin, S. T. Martin, M. D. Petters, F. D. Pope, and G. Rovelli. 2018. The viscosity of atmospherically relevant organic particles. *Nat. Commun.* 9 (1):956. doi: 10.1038/s41467-018-03027-z.

Rivera-Adorno, F., J. M. Tomlin, M. Fraund, E. Morgan, M. Laskin, R. C. Moffet, and A. Laskin. 2023. Inferring viscosity of individual substrate-deposited particles from assessment of their height-to-width ratios. *Aerosol Sci. Technol.* (In Press).

Saxena, P., and L. M. Hildemann. 1996. Water-soluble organics in atmospheric particles: A critical review of the literature and application of thermodynamics to identify candidate compounds. *J. Atmos. Chem.* 24 (1):57–109. doi: 10.1007/BF00053823.

Schill, S. R., D. B. Collins, C. Lee, H. S. Morris, G. A. Novak, K. A. Prather, P. K. Quinn, C. M. Sultana, A. V. Tivanski, K. Zimmermann, et al. 2015. The impact of aerosol particle mixing state on the hygroscopicity of sea spray aerosol. *ACS Cent. Sci.* 1 (3):132–41. doi: 10.1021/acscentsci.5b00174.

Shiraiwa, M., M. Ammann, T. Koop, and U. Pöschl. 2011. Gas uptake and chemical aging of semisolid organic aerosol particles. *Proc. Natl. Acad. Sci. USA.* 108 (27):11003–8. doi: 10.1073/pnas.1103045108.

Shiraiwa, M., Y. Li, A. P. Tsimpidi, V. A. Karydis, T. Berkemeier, S. N. Pandis, J. Lelieveld, T. Koop, and U. Pöschl. 2017. Global distribution of particle phase state in atmospheric secondary organic aerosols. *Nat. Commun.* 8 (1):15002. doi: 10.1038/ncomms15002.

Shiraiwa, M., and J. H. Seinfeld. 2012. Equilibration timescale of atmospheric secondary organic aerosol partitioning. *Geophys. Res. Lett.* 39 (24):2012GL054008. doi: 10.1029/2012GL054008.

Shiraiwa, M., A. Zuend, A. K. Bertram, and J. H. Seinfeld. 2013. Gas–particle partitioning of atmospheric aerosols: Interplay of physical state, non-ideal mixing and morphology. *Phys. Chem. Chem. Phys.* 15 (27):11441–53. doi: 10.1039/c3cp51595h.

Teimouri Sendesi, S. M., K. Ra, E. N. Conkling, B. E. Boor, M. Nuruddin, J. A. Howarter, J. P. Youngblood, L. M. Kobos, J. H. Shannahan, C. T. Jafvert, et al. 2017. Worksite chemical air emissions and worker exposure during sanitary sewer and stormwater pipe rehabilitation using cured-in-place-pipe (CIPP). *Environ. Sci. Technol. Lett.* 4 (8):325–33. doi: 10.1021/acs.estlett.7b00237.

Tomlin, J. M., K. A. Jankowski, F. A. Rivera-Adorno, M. Fraund, S. China, B. H. Stirm, R. Kaeser, G. S. Eakins, R. C. Moffet, P. B. Shepson, et al. 2020. Chemical imaging of fine mode atmospheric particles collected from a research aircraft over agricultural fields. *ACS Earth Space Chem.* 4 (11):2171–84. doi: 10.1021/acsearthspacechem.0c00172.

Virtanen, A., J. Joutsensaari, T. Koop, J. Kannosto, P. Yli-Pirilä, J. Leskinen, J. M. Mäkelä, J. K. Holopainen, U. Pöschl, M. Kulmala, et al. 2010. An amorphous solid state of biogenic secondary organic aerosol particles. *Nature* 467 (7317):824–7. doi: 10.1038/nature09455.

Wang, B., T. H. Harder, S. T. Kelly, D. S. Piens, S. China, L. Kovarik, M. Keiluweit, B. W. Arey, M. K. Gilles, and A. Laskin. 2016. Airborne soil organic particles generated by precipitation. *Nature Geosci.* 9 (6):433–7. doi: 10.1038/ngeo2705.

Wang, B., and D. A. Knopf. 2011. Heterogeneous ice nucleation on particles composed of humic-like substances impacted by O_3. *J. Geophys. Res.* 116 (D3):D03205. doi: 10.1029/2010JD014964.

Wang, B., A. T. Lambe, P. Massoli, T. B. Onasch, P. Davidovits, D. R. Worsnop, and D. A. Knopf. 2012. The deposition ice nucleation and immersion freezing potential of amorphous secondary organic aerosol: Pathways for ice and mixed-phase cloud formation: Ice nucleation by amorphous SOA. *J. Geophys. Res.* 117 (D16):n/a–/a. doi: 10.1029/2012JD018063.

West, C. P., A. C. Morales, J. Ryan, M. V. Misovich, A. P. S. Hettiyadura, F. Rivera-Adorno, J. M. Tomlin, A. Darmody, B. N. Linn, P. Lin, et al. 2023. Molecular investigation of the multi-phase photochemistry of Fe (III)–citrate in aqueous solution. *Environ. Sci. Process. Impacts.* 25 (2):190–213. doi: 10.1039/D1EM00503K.

Worsnop, D. R., J. W. Morris, Q. Shi, P. Davidovits, and C. E. Kolb. 2002. A chemical kinetic model for reactive transformations of aerosol particles: Reactive transformation of aerosol particles. *Geophys. Res. Lett.* 29 (20):57–1–57-4. doi: 10.1029/2002GL015542.

Wu, Z. J., J. Zheng, D. J. Shang, Z. F. Du, Y. S. Wu, L. M. Zeng, A. Wiedensohler, and M. Hu. 2016. Particle

hygroscopicity and its link to chemical composition in the urban atmosphere of Beijing, China, during summertime. *Atmos. Chem. Phys.* 16 (2):1123–38. doi: 10.5194/acp-16-1123-2016.

Zelenyuk, A., and D. Imre. 2009. Beyond single particle mass spectrometry: Multidimensional characterisation of individual aerosol particles. *Int. Rev. Phys. Chem.* 28 (2): 309–58. doi: 10.1080/01442350903037458.

Zelenyuk, A., and D. Imre. 2005. Single particle laser ablation time-of-flight mass spectrometer: An introduction to SPLAT. *Aerosol Sci. Technol.* 39 (6):554–68. doi: 10.1080/027868291009242.

Zelenyuk, A., D. Imre, J. Wilson, Z. Zhang, J. Wang, and K. Mueller. 2015. Airborne single particle mass spectrometers (SPLAT II & miniSPLAT) and new software for data visualization and analysis in a geo-spatial context. *J. Am. Soc. Mass Spectrom.* 26 (2):257–70. doi: 10.1007/s13361-014-1043-4.

Zhang, Q., J. L. Jimenez, M. R. Canagaratna, J. D. Allan, H. Coe, I. Ulbrich, M. R. Alfarra, A. Takami, A. M. Middlebrook, Y. L. Sun, et al. 2007. Ubiquity and dominance of oxygenated species in organic aerosols in anthropogenically-influenced Northern Hemisphere midlatitudes: Ubiquity and dominance of oxygenated OA. *Geophys. Res. Lett.* 34 (13):n/a–/a. doi: 10.1029/2007GL029979.

Zhang, Y., P. Liu, Y. Han, Y. Li, Q. Chen, M. Kuwata, and S. T. Martin. 2022. Aerosols in Atmospheric Chemistry. In *ACS In Focus*. Washington, DC, USA: American Chemical Society.

Zhao, R., A. K. Y. Lee, R. Soong, A. J. Simpson, and J. P. D. Abbatt. 2013. Formation of aqueous-phase α-hydroxyhydroperoxides (α-HHP): Potential atmospheric impacts. *Atmos. Chem. Phys.* 13 (12):5857–72. doi: 10.5194/acp-13-5857-2013.

Zhou, W., W. Xu, H. Kim, Q. Zhang, P. Fu, D. R. Worsnop, and Y. Sun. 2020. A review of aerosol chemistry in Asia: Insights from aerosol mass spectrometer measurements. *Environ. Sci. Process. Impacts.* 22 (8): 1616–53. doi: 10.1039/D0EM00212G.

Ziemann, P. J. 2003. Formation of alkoxyhydroperoxy aldehydes and cyclic peroxyhemiacetals from reactions of cyclic alkenes with O3 in the presence of alcohols. *J. Phys. Chem. A.* 107 (12):2048–60. doi: 10.1021/jp022114y.

Ziemann, P. J., and R. Atkinson. 2012. Kinetics, products, and mechanisms of secondary organic aerosol formation. *Chem. Soc. Rev.* 41 (19):6582–605. doi: 10.1039/c2cs35122f.